Atomistic computation of liquid diffusivity, solid-liquid interfacial free energy, and kinetic coefficient in Au and Ag

J. J. Hoyt[1] and Mark Asta[2]
[1]*Sandia National Laboratories, MS 1411, Albuquerque, New Mexico 87185*
[2]*Department of Materials Science and Engineering, Northwestern University, Evanston, Illinois 60208*
(Received 21 December 2001; published 3 June 2002)

Molecular-dynamics simulations using interatomic potentials of the embedded atom method have been performed on pure Ag and Au to compute materials parameters which are necessary for continuum modeling of dendritic solidification. The liquid state diffusion coefficient has been determined for temperatures in the vicinity of the melting points and good agreement with experimental data available for Ag is found. The kinetic coefficients for Au and Ag have been determined by monitoring the velocity of the solid-liquid interface as a function of undercooling. Rates of crystallization for the 100 and 110 directions agree well with a model proposed by Broughton, Gilmer and Jackson [Phys. Rev. Lett. **49**, 1496 (1982)] whereas the 111 direction exhibits a slower growth rate consistent with the presence of stacking fault clusters on the solid-liquid boundary, which anneal out during solidification. The solid-liquid interfacial free energy and its anisotropy have been obtained for Ag and Au by monitoring equilibrium fluctuations in the interface position. The fluctuation spectrum technique allows for an accurate determination of very small anisotropies in the interfacial energy and we find an anisotropy factor $1.0\pm0.3\%$ for Ag and $1.6\pm0.3\%$ for Au.

DOI: 10.1103/PhysRevB.65.214106 PACS number(s): 64.70.Dv, 81.30.Fb

I. INTRODUCTION

In recent years it has become evident that the phase field method is the ideal technique to model the complex morphologies that form during dendritic solidification. The advantage of the phase field model stems from the fact that the method was designed to circumvent the thorny numerical problem of tracking a sharp solid-liquid interface.[1] However, phase field modeling has progressed to such an extent that other numerical issues have been resolved as well. Karma and Rappel[2] have formulated the so-called thin interface limit and demonstrated that a much coarser finite difference grid may be used to model the interfacial region than was previously assumed. The resulting improved efficiency allowed the authors to study steady-state dendrite shapes and velocities in pure materials at intermediate undercoolings. At low undercoolings the length scales of the temperature field and the phase field differ by several orders of magnitude implying that conventional finite difference schemes are incapable of investigating this limit. Nevertheless, Plapp and Karma,[3] using a random walker technique, and Provatas *et al.*,[4] who employed an adaptive gridding algorithm, were able to bridge the two disparate length scales. In addition to the studies of dendritic solidification in pure materials, considerable progress has been made in the modeling of binary alloys.[5–8] Both free dendrite growth[9] and directional solidification have been investigated.[10,11] Despite the advances in phase field modeling, a major obstacle prevents the application of the technique to real alloy systems; namely, the specification of various materials-specific parameters that are required as input into the kinetic growth equations.

In the simplest formulation, Wheeler, Boettinger, and McFadden[5] noted that (in addition to bulk free energies) three parameters are required for each element to completely specify the quantities appearing in the phase field formulation of solidification. Assuming linear dependences on composition, these materials parameters are (1) the liquid state diffusion coefficient (D), (2) the solid-liquid interfacial free energy (γ), and (3) the kinetic coefficient (μ, the constant of proportionality between the velocity of crystallization and the undercooling). Furthermore, the microscopic solvability theory of dendrite growth[12–14] predicts that the shape and velocity of the dendrite is very sensitive to the small anisotropy of the solid-liquid interfacial energy. Using phase field simulations of dendrite growth in pure Ni, Bragard *et al.*[15] have demonstrated that the anisotropy of the kinetic coefficient can also play an important role in defining the operating state of the dendrite. Thus, accurate phase field models require experimental measurements or computational techniques sufficiently precise to extract the anisotropy of the relevant interfacial properties. Only a handful of experiments have successfully measured the anisotropy in γ (Refs. 16–22) and none have reported the anisotropy in μ. On the other hand, molecular-dynamics (MD) simulation techniques have been developed recently, which are capable of accurately computing all the necessary phase field parameters and their small anisotropies. In order to realistically model metal systems of interest in solidification, interatomic potentials of the embedded atom (EAM) form[23,24] have been employed in a number of MD studies. The EAM has proven very successful in modeling a broad range of structural, thermodynamic, and defect properties of noble and late transition metals and their alloys in both the solid and liquid state.[25,26]

Semiempirical EAM potentials have been applied previously in simulation studies of the liquid diffusivity. Alemany *et al.*[27,65] computed D for a variety of pure metals at a single temperature and Hoyt *et al.*[28] determined the diffusivity in Cu and Ni over a range of temperatures in the vicinity of the melting points. In addition to pure metals, solute diffusivities in the Ni-Al binary system have been computed by both Asta

et al.[29] and Alemany *et al.*,[30] the latter work demonstrating very good agreement with experiment. Hoyt *et al.*[31] have shown that a scaling law relating D to the excess entropy of the liquid[32–34] is obeyed for multibody EAM potentials in both pure and binary systems.

The EAM was employed recently in a MD study of the kinetic coefficient in pure Cu and Ni by Hoyt *et al.*[28] The value of μ obtained in these simulations was on the order of five times smaller than that used in previous phase field simulations of solidification of Cu-Ni alloys. Prior to this work by Hoyt *et al.*, several other MD studies have examined crystallization kinetics in a variety of elemental and alloy systems. A review of equilibrium and nonequilibrium MD methods used to extract μ can be found in Ref. 35. Broughton, Gilmer, and Jackson[36] (BGJ) studied crystallization in the Lennard-Jones system and formulated a collision-limited model for the growth rate of the solid (see also Burke *et al.*[37], Huitema *et al.*,[38] and Baez and Clancy[39]). Employing an analysis of equilibrium fluctuations in the number of solid and liquid particles in a coexisting two-phase system, Briels and Tepper[40] computed the 100 kinetic coefficient in the Lennard-Jones system and demonstrated good agreement with the forced-velocity MD method of BGJ. Very recently these authors also presented thorough comparisons of crystallization and melting kinetics employing nonequilibrium ''free-solidification'' MD simulations for model pair-potential systems.[41] Ishimaru *et al.*[42] employed the Tersoff[43] interatomic potential to examine the defect formation during the solidification of Si, and Clancy and co-workers[44,45] used both the Stillinger-Weber potential[46] and a tight-binding description to investigate crystallization kinetics in Si. Tymczak and Ray[47] reported melting and crystallization kinetics derived from a model pair potential for Na. Crystallization behavior in binary alloys[48–50,52] has also been studied via atomic-scale simulation. In particular, solute segregation at the moving solid-liquid boundary has been modeled for Si-Ge systems by Yu *et al.*,[48] and for Lennard-Jones mixtures by Celestini and Debierre.[50] The latter approach employs a nonequilibrium MD approach in which the system is ''pulled'' through a temperature gradient, analogous to directional-solidification experiments. This approach has recently been employed in the studies of crystallization kinetics in Au.[51]

In a recent MD study, Hoyt, Asta, and Karma[53] employed an analysis of the equilibrium fluctuation spectrum of the solid-liquid boundary to extract the interfacial free energy and its small anisotropy. The method has been utilized to determine γ in Ni, Cu,[54] and Al (Ref. 55) employing EAM potentials. The fluctuation spectrum is extremely sensitive to small anisotropies in the solid-liquid interfacial free energy. The approach described by Hoyt *et al.*,[53] therefore, provides estimates of the anisotropy with much lower statistical uncertainty than available from the values of γ derived in the pioneering work of Broughton and Gilmer.[56] These authors, who were the first to compute γ for a solid-liquid interface directly via MD, calculated values of the interfacial free energy for low-index interface orientations in the Lennard-Jones system employing a ''cleaving'' thermodynamic-integration technique. Recently Davidchack and Laird[57] have proposed a variant of the cleaving procedure for the hard-sphere system which yields anisotropy estimates with a statistical accuracy approaching that of the fluctuation technique.

In the present work the aforementioned MD methods are applied to derive all of the necessary phase field parameters in the metals Au and Ag. The structural and thermodynamic properties of both these elements are known to be described well by EAM potentials, and they are relevant to the study of solidification in that they are often used as components in filler materials for brazing applications. In addition, Ag and Au provide some opportunities to make comparisons with experiment as the liquid diffusivity in Ag has been measured[58] and the solid-liquid interfacial free energy for Au has been reported by Turnbull[59] and Jones.[60]

The paper is organized as follows. The following section outlines the numerical techniques employed in the MD simulations and describes the EAM potentials chosen for this study. The results section reports first the liquid diffusivities. Second, the growth velocity of the solid-liquid interface as a function of undercooling, and hence the kinetic coefficient, is reported. Here comparisons with the crystal-growth model of Broughton, Gilmer, and Jackson[36] are presented for the 100 and 110 growth directions. The distinctive features of the 111 direction are described in a subsequent section. Finally, we present the values and anisotropies of solid-liquid interfacial free energies, along with their associated statistical uncertainties, as derived from equilibrium fluctuation spectra measured in MD simulations.

II. NUMERICAL PROCEDURES AND THEORETICAL BACKGROUND

In recent MD studies of the solid-liquid interfacial free energy in Ni,[53,54] the sensitivity of the calculated values of γ to the details of the EAM potential were investigated. It was concluded that the calculated value of γ depends on the accuracy of the melting point predicted by the interatomic potential and the value of the anisotropy varied somewhat depending on the specific choice of the EAM potential. Those potentials which more accurately reproduced the elastic properties of the crystal yielded anisotropies in close agreement. In the present work the embedded atom potentials formulated by Voter and Chen[61] (VC) have been employed throughout. The Voter-Chen potentials are superior to the earlier versions due to Foiles, Baskes, and Daw[62] (FBD) in terms of the predicted elastic properties of the solid phase. The melting point of Au for the VC potential is closer to experiment than the FBD version whereas the melting point for Ag is slightly worse (see below).

There are two, formally equivalent, methods for computing the liquid state diffusion coefficient from MD simulations (e.g., Ref. 63). First, a well-known Einstein relation relates the long-time limit of the slope of the mean-square displacement of the atoms vs time to the diffusivity via

$$D = \frac{1}{6t}\langle |\mathbf{r}(t) - \mathbf{r}(0)|^2 \rangle. \tag{1}$$

The position of an atom at any time t is written as $\mathbf{r}(t)$ and the angular brackets denote an average with respect to all atoms in the MD simulation and over all time origins. Alternatively D can be computed through an integration of the velocity autocorrelation function (VACF), employing the Green-Kubo relation

$$D = \int_0^\infty Z(t)\,dt, \tag{2}$$

where $Z(t) = (1/3)\langle \mathbf{u}(t) \cdot \mathbf{u}(0) \rangle$ and $\mathbf{u}$ is the velocity of an atom. In the results to follow, the diffusion coefficient was determined by integration of the $Z(t)$. For run times, systems sizes and homologous-temperature ranges comparable to those employed in the present study, we have found in previous studies that the two methods for computing D typically differ by less than 3%. In the simulations periodic cells of 2048 atoms were employed. After an equilibration of $\approx$50 ps, runs were performed in the microcanonical ensemble with a time step of 1 fs. Total sampling times of 100 ps were found to be sufficient to lead to well-converged values for the VACF.

Computation of the kinetic coefficient was performed using a procedure described previously.[28] Periodic simulation cells of dimensions $24\times10\times10$ unit cells (9600 atoms) were generated with the 100 crystal directions coincident with the Cartesian coordinate axes. (For the kinetic coefficient along the 110 directions, cells with similar spatial dimensions were employed while for 111 significantly larger cells were used owing to a pronounced size effect for this orientation as discussed below.) Approximately three quarters of the long dimension was melted and the remaining atoms were held fixed. The resulting solid-liquid system was then equilibrated at the melting point. Solidification was initiated by bringing the system to temperatures below the melting point and allowing the simulation to proceed under constant N-P-T conditions. The position of the interface vs time was determined by monitoring the total enthalpy of the solid-liquid system and comparing with the enthalpies determined separately for the bulk solid and liquid phases. The procedure is described in detail in Ref. 28. A total of nine undercoolings were investigated, the largest being 200 K. For the lowest undercoolings (10 K), runs of 140 ps were required to accurately determine the velocity. A time step of 2 fs was employed in the simulations. The computation of the kinetic coefficient also allows for a determination of the melting point for the EAM potentials by identifying that temperature at which the interface velocity is zero. The knowledge of the melting point is necessary for the calculation of the interfacial free energy.

The solid-liquid interfacial free energy for Au and Ag was determined by the procedure outlined in Ref. 53. For a two-dimensional solid-liquid system the interface fluctuation spectrum is given by

$$\langle |A(k)|^2 \rangle = \frac{k_B T}{Wb(\gamma + \gamma'')} \frac{1}{k^2}, \tag{3}$$

where $A(k)$ is the Fourier transform of the interface amplitude as a function of position along the interface and the angular brackets denote equilibrium values (corresponding to an average of many configurations). The quantity W is the total length of the solid-liquid boundary, b is the thickness of the system, and $k_B T$ has the usual meaning of Boltzmann's constant times the absolute temperature (for elemental systems T in the above equation corresponds to the bulk melting temperature). The term $\gamma + \gamma''$ is known as the stiffness and γ'' is the second derivative of the solid-liquid energy as a function of the angle of the average interface normal. As explained previously[53] the stiffness is an order of magnitude more anisotropic than γ itself and thus small anisotropies can be extracted accurately from fluctuations in the solid-liquid boundary as determined from MD simulations.

In the present study periodic cells of dimensions $W \times 2W \times b$ were used, where W is on the order of 250 Å, the long dimension ($2W$) is normal to the solid-liquid boundary and the thickness b is three unit cells. Half of the $2W$ dimension was melted and subsequently the system was equilibrated at the melting temperature. During the equilibration stage the dimensions of the cell parallel to the solid-liquid interfaces were constrained at values dictated by the zero-stress lattice constants of the crystalline phase at its melting point. The length normal to the interface was allowed to equilibrate to minimize the stress in the bulk liquid and solid portions of the cell. Subsequently, the amplitude vs position of the two solid-liquid interfaces was extracted every 100 time steps (0.2 ps) for a minimum of 400 ps employing a microcanonical ensemble. This data was used to compute the equilibrium values and statistical uncertainties of the Fourier amplitudes $A(k)$ from which the stiffness is readily derived using Eq. (3). The method used to distinguish between solid and liquid atoms and the procedure for identifying the interface boundary are described in detail in a previous publication.[53]

III. RESULTS AND DISCUSSION

The diffusion coefficient

The diffusion coefficient vs temperature in the range 1050–1450 K is shown in Fig. 1 for both Au and Ag. The Au results are given by the filled squares whereas the data for Ag are denoted by filled circles. As discussed below the melting points for these potentials are 1115 K and 1120 K for Ag and Au, respectively. Thus the two data points at the low-temperature end of Fig. 1 refer to liquids in the undercooled state. The trend with temperature is nearly linear for this temperature range and the slope of the Ag curve ($6.04 \times 10^{-}8$ cm^2/s/K) is slightly higher than that of Au ($3.77 \times 10^{-}8$ cm^2/s/K). The trend with temperature is similar in magnitude to that observed for Cu and Ni in Ref. 28.

The open circles in Fig. 1 are the experimental data of Yang *et al.*[58] for Ag who employed a capillary reservoir technique and radioactive tracers. The agreement with the VC-EAM is quite good, differing by at most 20% over the entire temperature range.

In Fig. 1, the points inscribed with the symbol "×" denote the results of Alemany *et al.*[27] Since the Alemany *et al.*

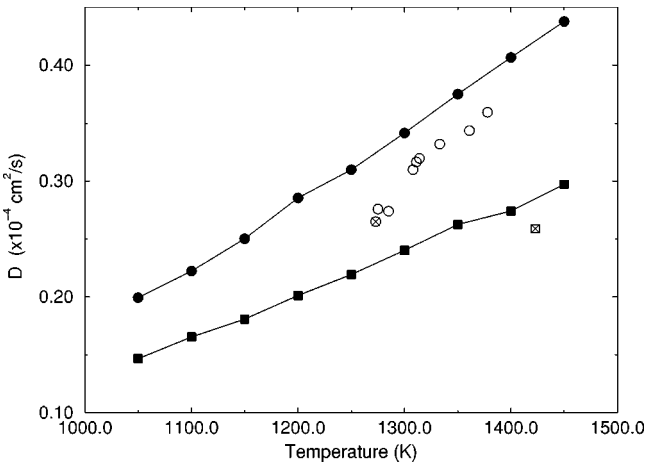

FIG. 1. The diffusion coefficient vs temperature in the vicinity of the melting points as determined from MD simulations using the VC-EAM potential. Results are shown for liquid Ag (filled circles) and liquid Au (filled squares). The open circles are the experimental data of Yang *et al.* (Ref. 47) and symbols with "×" are the MD results of Alemany *et al.* (Ref. 26)

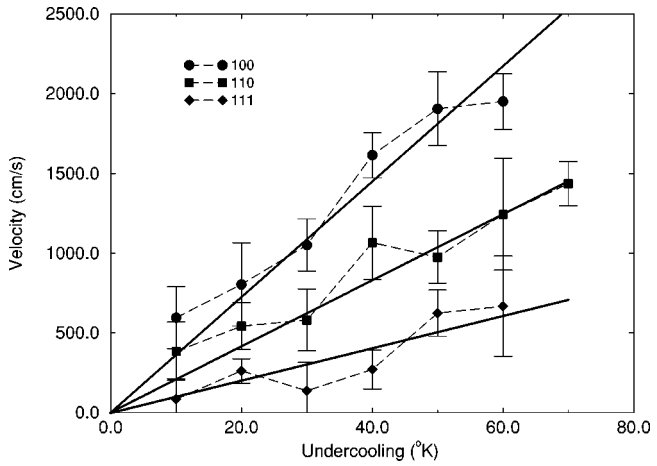

FIG. 2. Velocity of the solid-liquid boundary as a function of undercooling in pure Au for the low-index directions 100, 110, and 111. The slopes of the curves at the low undercoolings shown by the heavy solid lines yield the kinetic coefficients.

study also used VC potentials, it is unclear why a discrepancy exists between the two computed values of D. The difference is not large, only 10% for Au and 20% for Ag. There are three main differences between the two simulations: the number of atoms used in the MD runs differed, the time step was smaller by a factor of 2 in the present study and the Alemany *et al.* simulations were performed at the experimental density as opposed to the EAM computed density (as was done here). Nevertheless, we have performed an additional simulation for Au at exactly the conditions of the Alemany *et al.* study and the 10% discrepancy remains. Therefore, we suspect that the observed differences results from a slightly different fit of the potential to the VC scheme. The fitting procedure involves varying parameters of the embedding, the density, and the pair-potential functions such that a best fit to a variety of experimental properties is achieved. The fit is constructed such that the lattice parameter, the cohesive energy, and the bulk modulus are all reproduced exactly, the remaining experimental quantities include elastic constants and the energy of formation of a vacancy. As pointed out by Voter,[64] the notion of a best fit involves some degree of subjectivity and we believe a slightly different potential fit is the source of the discrepancy observed in Fig. 1.

To support the idea that the difference in D observed is due to a slightly different potential set, we have reproduced the results for Ni reported in an earlier paper by the Alemany group[65] where the VC-EAM form was also used. The advantage of checking the Ni results is that the parameters of the Voter-Chen potential are given explicitly in Ref. 61 and thus one can be sure that the exact form of the potential is consistent. Reproducing the Alemany *et al.* simulation ($D=0.0781$ Å^{-3} and $T=1875$ K), we find a result that differs by less than 2% from the quoted value in Ref. 65. Therefore, the discrepancy of Fig. 1 cannot be the result of numerical implementation and most likely stems from a different potential.

The kinetic coefficient, 100 and 110 interfaces

The melting point for the EAM potentials can be found by monitoring the solid-liquid interface velocity vs temperature and extrapolating to the temperature corresponding to zero motion. With this procedure we find the melting point for Ag to be 1115 K and 1120 K for Au. These values are below the actual measured melting points of 1234 K and 1338 K for Ag and Au, respectively, but the agreement with experiment is reasonable given that no properties of the liquid were utilized in the potential fit procedure. For comparison, the melting points for the Foiles, Baskes, and Daw EAM potentials are 1170 for Ag and 1090 for Au.[66]

Figure 2 shows the interface velocity vs undercooling for the 100, 110, and 111 interfaces as determined for Au. The linear relationship $V=\mu\Delta T$ is seen to be obeyed fairly well. The error bars on the velocities shown in Fig. 2 were determined by first converting the computed potential energies vs time into the rate of change of the solid phase length (Ref. 28) and subsequently determining the frequency with which statistically independent data is sampled. Let $y(t)$ represent the solid length as a function of time where the data is collected over small time steps in the simulation (0.05 ps) and let $\hat{y}(t)$ be the length predicted by a linear least-square fit to all the data. Then the correlation function given by $\langle[y(t)-\hat{y}(t)][y(0)-\hat{y}(0)]\rangle$ was monitored and the characteristic time t_c, over which the function decays to zero, was obtained. Since t_c represents the time over which fluctuations in the solid-liquid interface position [relative to the deterministic value $\hat{y}(t)$] becomes uncorrelated, a complete data set was then averaged over blocks of length t_c and the uncertainties were determined by standard linear regression analyses. The error bars in Fig. 2 represent estimated values for the standard error σ. As explained below, we find the uncertainties for the lowest undercoolings to be somewhat larger than the high-velocity points.

In Fig. 2, the best fit slopes of the solid lines yield the kinetic coefficient and for Au we find $\mu_{100}=36.3\pm3.6$, $\mu_{110}=20.7\pm2.4$, and $\mu_{111}=10.1\pm2.7$ in units of cm/s/K

(where uncertainties represent 95% confidence levels). These values and uncertainties for μ were obtained from a linear-regression analysis of the velocity-undercooling data up to $\Delta T = 60$ K. As in Ref. 28, the ratio of $\mu_{100}/\mu_{110} = 1.75 \pm 0.27$ is found to be comparable to the ratio of d spacings of the 100 and 110 planes ($\sqrt{2}$), while the ratio of μ_{100}/μ_{111} is ≈ 4. As discussed below, the values of μ for the 100 and 110 interfaces are consistent with a model originally proposed by BGJ.[36] However, the kinetics of the 111 interface are distinct from the mechanisms embodied in the BGJ model and this special case is discussed in the following section.

In 1982, BGJ argued that the crystallization rate as a function of temperature can be written as

$$V = \frac{d}{\lambda}\left(\frac{3k_BT}{m}\right)^{1/2} f_o e^{-\Delta S/k}(1 - e^{-\Delta G/k_BT}). \qquad (4)$$

In this equation the rate at which atoms attempt jumps from the liquid to the solid is given by the thermal velocity, $(3k_BT/m)^{1/2}$, divided by the average distance traveled by the atom, λ. The authors argue that $\lambda = 0.4d$ where d is the interatomic spacing. The thermal velocity consists of Boltzmann's constant times the temperature, k_BT, and m, the atomic mass. In the BGJ expression f_o represents the fraction of atomic jumps that are successful in producing an atom of the solid phase. The prefactor f_o can also be defined as the ratio of the number of favorable attachment sites on the interface to the total number of crystal sites. The driving force for crystallization in the BGJ model is reflected by the quantities ΔS, the entropy difference between the liquid and solid, and ΔG, the difference in Gibbs free energy. The BGJ model differs from the earlier growth models proposed by Wilson[67] and Frenkel[68] in that the rate-limiting factor is the thermal velocity of the atoms rather than the liquid-diffusion coefficient. BGJ conclude that such a replacement is necessary due to the fact that the measurable rates of crystallization were found in MD simulations for the Lennard-Jones sytems at temperatures well below the glass transition temperature, i.e., where D is effectively zero.

The BGJ model falls into the category of what Turnbull[69] has denoted a collision-limited growth model. As reviewed in a recent paper by Jackson,[70] the velocity predicted by Eq. (4) is expected to be valid for those materials and interface orientations for which a significant altering of the atomic structure near the solid-liquid boundary is not required. Examples of systems which meet this restriction are simple metals and model systems which can be described by angular independent central force atomic potentials. The EAM systems studied in the present work are also expected to fall into the collision-limited growth category. Materials which are characterized by strongly covalent bonding, such as Si, require significant structural rearrangement upon crystallization. For this class of materials the original Wilson-Frenkel theory has been shown to be more appropriate.

The BGJ expression can be compared directly to the results for Au and Ag obtained here and to the results of Cu and Ni determined in Ref. 28. At small undercooling, The $-\Delta G/k_BT$ term appearing in Eq. (4), can be written as $(L/k_BTT_M)\Delta T$, where L is the latent heat and T_M is the melting temperature. Furthermore, the entropy contribution can be taken as independent of temperature and thus $\Delta S = L/T_M$. Since L can be easily found in MD simulations the only unknown appearing in the BGJ velocity equation is the parameter f_o. However, BGJ used f_o as an adjustable parameter, derived a best fit of Eq. (4) to their MD results on the Lennard-Jones system and found $f_o = 0.27$. In the results to follow, we shall use the BGJ fit value of f_o and thus there are no free parameters in the comparison.[71] However, a very important simplification needs to be noted at this point. In the model-simulation comparison we are assuming, the value of f_o is independent of the growth direction. The assumption is merely one of convenience since, at present, there does not exist any theoretical prediction for the value of this factor nor its anisotropy. As discussed below a more thorough understanding of the quantity f_o may be critical in explaining the observed orientation dependence of the crystallization rate.

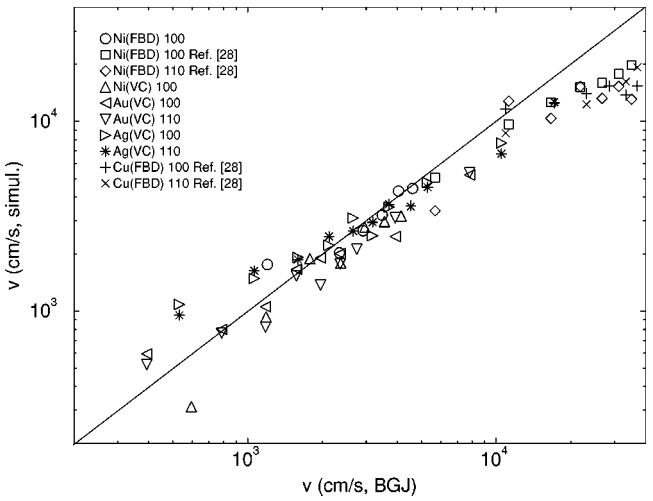

FIG. 3. Comparison of crystal-growth rates obtained from simulation to that predicted by the BGJ model. Included in the comparison are results for Ag and Au, low undercooling MD data using two different EAM potentials for Ni and high undercooling data from Cu and Ni (Ref. 27).

Figure 3 shows the velocity predicted by the BGJ model vs the interface velocity measured in MD simulations for 100 and 110 solid-liquid interface orientations. Several data sets are depicted. The Au and Ag results are from the present study and the Cu and Ni results at large undercooling are from Ref. 28. Additional simulations were also performed for Ni at lower undercoolings ($\Delta T < 70$ K) and are included in the results of Fig. 3. Finally, for completeness, two separate EAM Ni potentials were simulated at low undercoolings, the VC Ni form and the Foiles Baskes Daw (denoted FBD) Ni potential.

At the lowest undercoolings, i.e., smallest velocities, the agreement between MD results and the BGJ model is good, however there is sizable scatter in the data. We attribute this scatter to at least two effects. First, the melting points as determined above contain some uncertainty. Uncertainty in T_M has the largest effect on the computed velocities at very small undercoolings. Second, low undercoolings correspond

to the low velocities of solidification and even during long MD runs the solid-liquid boundary advances only a few atomic planes. The slow growth will thus increase the statistical uncertainties in the energy vs time behavior from which the velocity is extracted.

Up to relatively large undercoolings of about $\Delta T = 500$ K, the agreement between the BGJ model and simulation results is very good. It should be emphasized that, assuming f_o is roughly the same for both orientations, Eq. (4) predicts that the ratio of μ for 100 and 110 interface orientations is the ratio of the interplanar spacings, or $\sqrt{2}$. The simulation results shown in Fig. 3 appear to be generally consistent with this prediction. The result is important from the point of view of solidifcation studies, as it suggests that the anisotropy of μ, defined as $(\mu_{100}-\mu_{110})/(\mu_{100}+\mu_{110})$, is roughly 17% for simple elemental fcc-based metal systems.

As shown in Fig. 3, at very high undercoolings, the BGJ model significantly overestimates the crystallization velocity. Although the undercoolings, where the discrepancy sets in, are too high to be relevant for comparison with experimental studies of solidification, it is, nevertheless, of interest to speculate as to the origin of the deviation between simulation and model. One possible origin is the linear relationship between the thermodynamic quantities in Eq. (4) and the undercooling. At large undercooling this approximation may no longer be valid. However, one can extend the approximation for ΔG to a term involving ΔT^2, the coefficient of the higher-order term depends on the heat capacity. We find that the inclusion of this correction cannot account for the discrepancy observed in Fig. 3. Another intriguing possibility for the discrepancy in Fig. 3, is a roughening transition in the vicinity of $\Delta T = 500$ K. The BGJ model assumes that the solid-liquid interface is rough. For a smooth interface where attachment sites on the crystalline face are not readily available, one would expect the crystallization rate to slow. In particular, associated with a smoother interface would be expected a lower value of the prefactor f_o in Eq. (4) which represents the fraction of available sites for attachment to the interface. Although the downturn in the data of Fig. 3 at high V is, at present, not understood, it should be pointed out that the effect has been observed previously. In their study of Na, Tymczak and Ray[47] present MD simulation data (their Fig. 4) which also demonstrates that the BGJ model overestimates the velocity at undercoolings greater than about 100 K.

The kinetic coefficient, 111 interface

Although the BGJ model of crystallization kinetics is obeyed quite well for the 100 and 110 orientations, the agreement between the model and simulation results is poor for 111 interfaces. Typically, the MD results for fcc metals show a much lower velocity than that predicted by Eq. (4). Specifically, if we assume that f_o depends relatively weakly on orientation, the BGJ model predicts that the 111 velocity should be, in fact, higher than that of 100 (since the interplanar spacing for 111 is larger than for 100). In 1988 Burke, Broughton, and Gilmer[37] (BBG) investigated the kinetics of crystallization in the Lennard-Jones system for the 100 and 111 interfaces and proposed an explanation as to the slower-than-expected growth in the 111 direction. The authors argue that an atom from the liquid phase can attach itself to either an fcc site or an hcp site on the adjacent 111 solid surface. If the stacking-fault energy is sufficiently low and/or the driving force sufficiently high, islands of defective hcp atoms may form during the course of solidification. Since, away from the interface the crystallized solid is found to be free of stacking-fault defects, BGJ argue that the system must ''anneal'' out these hcp islands in order for the crystallization to proceed. Thus there appears a thermally activated step in the growth of 111 interfaces, not present in the BGJ model, required for the conversion of all layer atoms to the fcc orientation. As discussed below, we find evidence supporting the explanation of Burke *et al.* for the case of the low-stacking-fault-energy metals Au and Ag modeled in the present study.

Evidence for the existence of growth affected by the annealing of stacking faults is a strong dependence of the simulated crystallization rate upon the system size. BBG found that the 111 growth velocity is faster for a periodic system in which the area of the solid-liquid interface is decreased. The authors argue that, in a system with small periodic lengths parallel to the interface, the defect clusters cannot grow as large before contacting clusters from the periodic image of the cell. Since it is the cluster circumference to area ratio that determines the rate of annealing, smaller systems exhibit a higher growth rate. In the present study we investigated the size dependence of the 111 growth velocity for Au, finding results similar to those observed for the Lennard-Jones system by BBG. Specifically, we calculated the 111 growth velocity vs undercooling for both a relatively small system, whose solid-liquid boundary area measured 1728 Å^2 [seven $(1\bar{1}0)$ atomic planes by four $(11\bar{2})$ planes], as well as a larger system with an interface area of 5876 Å^2 [$12(1\bar{1}0) \times 8(11\bar{2})$]. Consistent with the findings of BBG, the smaller system size possesses a growth rate in the 111 direction which is roughly 50% higher than that for the large system. No such size effect was found for the 100 or 110 growth directions.

The evidence that the BBG mechanism is operative for the case of Au and Ag is provided by a detailed examination of the structure of the solid-liquid boundary. In what follows, it will be convenient to distinguish atoms of the solid phase from atoms belonging to the liquid phase. For this purpose we have employed the technique introduced in Ref. 53 where a structural ''order parameter'' can be assigned to each atom. The order parameter is found from the mean-square displacement of the 12 nearest neighbors from the ideal sites of the underlying crystalline lattice. For numerical values of the parameter below ≈ 0.7 the atom is considered as part of the fcc solid phase. In the case of the 111 orientation, order-parameter values above this cutoff indicate that the atom is either part of the liquid phase, or part of an hcp defect cluster on the solid surface, as discussed below. Figure 4 shows a cut parallel to the solid-liquid interface at a depth well within the solid phase. The figure was generated from the large solid-liquid system of pure Au. In Fig. 4, and subsequent

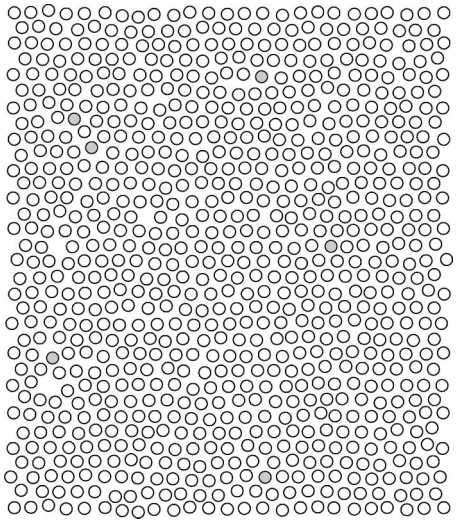

FIG. 4. Plane of atoms parallel to the solid-liquid boundary but located well within the solid phase. The white atoms are those which belong to the solid phase whereas the gray atoms denote liquidlike or ''defect'' atoms. Deep within the solid phase there exist only a few defective atoms.

Figs. 5 and 6, the white atoms denote solid atoms, whereas the gray atoms are liquid or defect atoms. The crystalline plane clearly shows the sixfold symmetry of the 111 plane and at this position far from the boundary plane there a very few gray ''defect'' atoms. Figure 5 depicts a similar plane at a position in the liquid far from the solid-liquid interface. The thickness of the cut was kept the same as in the previous figure. In this position the atomic arrangement is highly disordered, there is little evidence of sixfold symmetry and most atoms are colored gray. The preceding figures should be compared with Fig. 6 that shows the atomic arrangement for the layer adjacent to the liquid phase. Here roughly half of the atoms are white and exhibit sixfold symmetry. These atoms occupy the proper lattice positions of the crystallizing

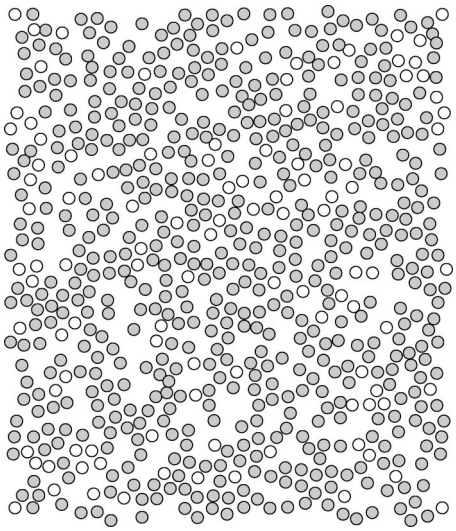

FIG. 5. Plane of atoms parallel to the solid-liquid boundary but located well within the liquid phase. Most of the atoms are liquidlike and no sixfold symmetry is observed.

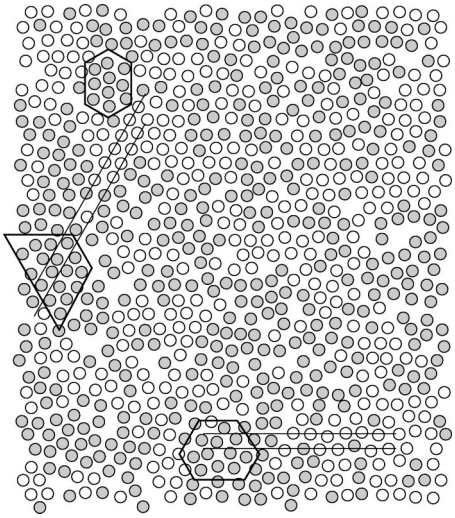

FIG. 6. Plane of atoms at the solid-liquid interface. Clusters of defect (i.e., gray) atoms are observed which possess sixfold symmetry as indicated by the heavy solid lines. Such regions represent stacking faults as can be seen by the offset of the atom planes from the perfect fcc configuration (the light solid lines).

solid. However, there are also many other atoms which also exhibit sixfold symmetry, but, being colored gray, do not lie close to perfect fcc sites. These atoms represent defect clusters on the surface and three such regions are shown by heavy black lines in Fig. 6. For the regions in the lower central part of the figure and for the area to the left of the drawing, one can show that the atomic arrangement is hcp by extending the fcc atom planes in nearby regions as shown by the light black lines. The displacement of the gray atoms from the ideal planes (white atoms) is one-half of the $1\bar{1}0$ d spacing as expected from a stacking fault. The continued crystallization of the system requires that the faulted regions as shown in Fig. 6 must shrink at the expense of the perfect fcc regions and as a result the 111 kinetics is slower relative to the 100 and 110 orientations.

The region delineated in the upper left portion of Fig. 6 shows a sixfold symmetric arrangement of gray atoms, yet the region is rotated by 30 deg with respect to the underlying 111 surface. Such a rotation implies that there are alternate atoms in the fcc and hcp positions in the defect cluster and the nearly equal atom spacing means that there exists some displacement of atoms from the hollow sites. Although the region is an interesting observation, it is doubtful that such defect clusters play a major role in the growth kinetics, as they appear to occur infrequently.

The presence of stacking-fault islands does not seem to fully explain the discrepancy between the simulated velocity vs undercooling behavior and the growth model of BGJ assuming an orientation-dependent value for f_o. The fast growth rate of the small system size, which minimizes the effect of stacking-fault formation, is still much less than that predicted by BGJ. Recall from Eq. (4) with constant f_o that the crystallization rate is proportional to the interplanar spacing d meaning that the 111 orientation ($d=\sqrt{3}a/3$) should solidify more rapidly than the 100 orientation ($d=a/2$). The relationship $\mu_{111}>\mu_{100}$ has never been observed in atomistic

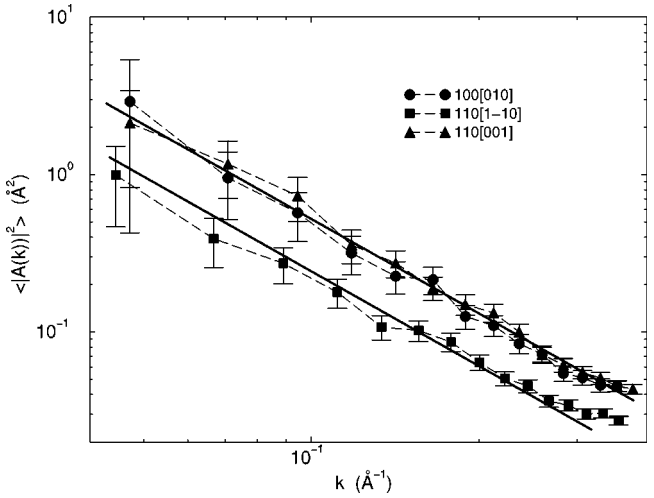

FIG. 7. Fluctuation spectra for Au for the three orientations 100[010], 110[1$\bar{1}$0], and 110[001]. The data exhibit the slope of -2 predicted by theory as indicated by the heavy solid lines.

simulations of fcc metals even for very small system sizes. Huitema *et al.*[38] offer an alternative explanation for the slow growth of the 111 direction. These authors argue that the kinetic coefficient consists of two mechanisms that add in series, i.e., $1/\mu = 1/\mu_{org} + 1/\mu_{hop}$. Here ''org'' refers to the mechanism of intralayer organization of the liquid atoms into the crystalline lattice and μ_{hop} denotes the rate of hopping within the layer to increase the density. From a detailed examination of their simulations of crystallization in the Lennard-Jones system the authors find that the dominant mechanism in the 100 direction is the μ_{org} term, whereas the hopping contribution is large for the 111 direction. The BGJ model assumes a mechanism of atom attachment from the liquid to the solid neglecting any mechanism of the type μ_{hop}. Although the Huitema *et al.* arguments provide a plausible explanation for the observed behavior, the theory is at this point qualitative and a fully quantitative description of the crystallization of the 111 orientation remains an open question. An additional consideration for the behavior of 111 growth is as follows. As noted above the comparison of theory with simulation results assumed the f_o parameter appearing in the BGJ model is isotropic. A complete theoretical treatment of the f_o term, including its dependence on crystallographic orientation, may be required to fully explain the crystallization kinetics of fcc metals along 111 growth directions.

The solid-liquid interfacial free energy

Figure 7 depicts the equilibrium fluctuation spectra of the solid-liquid interface for Au as obtained by MD simulations (described above) for three different orientations of the simulation cell. The figure plots on a log-log scale the quantity $\langle |A(k)|^2 \rangle$ vs the wave number k. The orientations are denoted by two sets of numbers. The first triplet of integers refers to the crystal face which is adjacent to the liquid, whereas the second set denotes that crystallographic direction which runs along the interface in the quasi-2D (two-dimensional) simulations (see above). In the figure the heavy black lines illustrate a slope of -2 as is predicted from the capillary theory result of Eq. (3). Except for the data points at low k with high statistical uncertainties, the slope of the MD data agrees very well with the theoretical value. The offset of the three curves from one another reflects the fact that the orientations are of different stiffnesses, although in this case the 100[010] and 110[001] orientations have nearly identical values of $\gamma + \gamma''$. Using Eq. (3), the stiffnesses are found to be 96 ± 5 for the 100 [010] configuration, 155 ± 9 for 110[1$\bar{1}$0], and 93 ± 4 for 110 [001] in units of mJ/m^2 (where all error estimates reported here and below represent 95% confidence limits).

The uncertainties quoted in this section were derived from a standard analysis based on estimates of the relaxation times of the fluctuations as a function of wave number. Specifically, utilizing the fact that the fluctuation amplitudes are governed by a Gaussian distribution, the variance in the mean value of $\langle |A(k)|^2 \rangle$ is given as $2\langle |A(k)|^2 \rangle^2 \tau(k)/t_{run}$, where t_{run} is the length of the MD simulation (e.g., Ref. 63). The quantitity $\tau(k)$ is the relaxation time of fluctuations with a given wave number k, and is estimated by fitting an exponential decay in time to the calculated values of the autocorrelation functions $\langle A(k,t)A(-k,0) \rangle$ derived from the MD data. Assuming the fluctuation kinetics are governed by random atom attachment-detachment kinetics, $\tau(k)$ is expected to display a quadratic dependence on k.[75] This relation allowed estimates of τ to be obtained for the lowest wave numbers from the data from high and intermediate values of k where the short relaxation times lead to reasonable statistics in the calculation of the time correlation functions. Values of τ were found to range from roughly 1 ps for the largest wave numbers considered in the simulations to more than 400 ps for the smallest value of k. In deriving interface stiffnesses from the data shown in Fig. 7, we excluded values of $\langle |A(k)|^2 \rangle$ for those wave numbers for which τ was more than one-tenth of the total simulation time.

As outlined previously,[53,54] the stiffness values for three different orientations can be used to parametrize γ for all orientations (assuming an analytic interfacial free energy with small anisotropies). The procedure involves expanding γ in terms of Kubic harmonics, i.e., those terms of an expansion in spherical harmonics which retain the cubic symmetry of the crystalline solid, as follows:

$$\gamma(\hat{n})/\gamma_o = 1 - 3\epsilon + 4\epsilon \sum_{i=1}^{3} n_i^4 + \eta \left(\sum_{i=1}^{3} n_i^6 + 30 n_1^2 n_2^2 n_3^2 \right) + \cdots . \quad (5)$$

In the above expression, the n_i represent the components of the normal vector to the solid-liquid plane. By evaluating the stiffness ($\gamma + \gamma''$) from Eq. (5) and using the results of Fig. 7, the three parameters γ_o, ϵ, and η can be determined. As discussed in Ref. 31 the expansion of γ up to the terms appearing in Eq. (5) is well converged, i.e., the expansion correctly predicts the stiffness for other orientations as measured by the fluctuation spectra.

Table I lists the γ_o and the anisotropy parameters ϵ and η for VC Au and Ag. The value of $\gamma_o = 126 \pm 11$ mJ/m^2 can be

TABLE I. Solid-liquid interfacial free energies and associated anisotropy parameters calculated for Ag and Au from simulated fluctuation spectra. Error estimates represent 95% confidence levels.

	γ_o (mJ/m^2)	ϵ	η	$(\gamma_{100}-\gamma_{110})/2\gamma_o$(%)
Ag	112 ± 5	0.016 ± 0.003	-0.015 ± 0.003	1.0 ± 0.3
Au	126 ± 5	0.018 ± 0.003	-0.007 ± 0.003	1.6 ± 0.3

compared with the value for Au estimated by Turnbull from supercooling data, $\gamma_o=132$ mJ/m^2. The excellent agreement with the Turnbull result may be somewhat fortuitous since the melting point for Au is underestimated with the VC potentials. Thus, as discussed in Ref. 53, the interfacial energy derived from a more accurate potential would likely be somewhat higher than the 126 mJ/m^2 value obtained here. On the other hand, the Turnbull value represents a lower limit on γ_o and overall agreement with experiment is adequate. Jones[60] has reported the solid-liquid interfacial free energy for a number of pure metals and quotes $\gamma_o=270$ mJ/m^2 for Au. At this point it is unclear why there exists a large discrepancy between the value given by Jones and the two results quoted above.

For completeness we note that Ewing[72] has proposed a simple model for the solid-liquid interfacial free energy and, when applied to Au, yields a value of $\gamma_o=148$ mJ/m^2. Despite the good agreement with the present result, recent simulations indicate that the Ewing model is not a valid description of the solid-liquid interface. Ewing obtains γ_o using a simplified picture of the liquid structure under the assumption that the crystal face adjacent to the liquid remains completely planar. Heni and Lowen[73] have determined the interfacial energy in the hard-sphere system for a liquid in contact with a featureless rigid wall and found an energy of $\gamma_o=2$ in reduced units. This energy is well above the value for the solid-liquid interfacial energy in the hard-sphere system ($\gamma_o\approx0.62$, Ref. 57), suggesting that the planar crystal face assumption is inappropriate. Furthermore, the Ewing model result predicts that the excess energy of the solid-liquid boundary accounts for roughly one-half of γ_o, the remainder being the entropic contribution. A large excess energy contradicts a recent proposal by Laird[74] who suggested that for most elemental metals the solid-liquid interfacial free energy is almost completely entropic, i.e., $E_{xs}\approx0$. In light of these more recent studies it would appear that the good agreement between the Ewing result and the present study is purely coincidental.

From the point of view of dendritic solidification the important parameter of Table I is the anisotropy given by $(\gamma_{100}-\gamma_{110})/2\gamma_o$. The anisotropy values for Au and Ag are in the same range, 1%–2%, as those computed for Cu and Ni (Ref. 53) with Ag being the lowest. The fact that $\gamma_{100}>\gamma_{110}$ for Au, Ag, Cu, and Ni is consistent with theoretical predictions and experimental observations of the preferred crystallographic growth direction observed during dendritic solidification. In addition, a positive value of the anisotropy is also found in all the available experimental observations, see Refs. 16–22. Thus, it is interesting to note that Davidchack and Laird[57] report that the anisotropy for the hard-sphere system is on the order of 1.5%, but is *negative*. The physical origin of the difference in sign remains to be seen, but is most likely due to the lack of an enthalpy contribution in the hard-sphere case.

IV. CONCLUSIONS

Several materials parameters necessary for continuum modeling of dendritic solidification are very difficult to obtain experimentally and it is now apparent that atomistic modeling can supply estimates to these quantities. In this work we have obtained from MD simulations the liquid-state diffusion coefficient, the kinetic coefficient, and the solid-liquid interfacial free energy for pure Au and Ag. Importantly, the simulation techniques described in the present work provide a means for extracting statistically accurate values of the small anisotropies of the latter two quantities. The computed diffusion coefficient as a function of temperature agrees well with the experimental data available for Ag. The calculated crystal growth rates in the 100 and 110 directions are well described by the Broughton, Gilmer, and Jackson[36] model of collision-limited growth. Associated with the slower-than-expected growth rate of the 111 orientation is the presence of stacking-fault clusters at the solid-liquid interface during crystallization, consistent with the findings for Lennard-Jones systems by Burke, Broughton, and Gilmer.[37] An experimental result due to Turnbull[59] of the solid-liquid interfacial free energy for Au agrees well with the value of γ_o computed using the fluctuation spectrum technique in the present study, while the additional experimental result of Jones[60] shows a large discrepancy with these estimates. The important anisotropy factors for the solid-liquid interfacial free energy were found to be $1.0\pm0.3\%$ for Ag and $1.6\pm0.3\%$ for Au. These values are comparable to those derived in related simulation studies for the fcc metals Cu, Ni, and Al,[31,53,55] as well as a recent experimental estimate for an Al-Cu alloy.[22]

ACKNOWLEDGMENTS

The authors wish to thank Professor A. Karma for many helpful discussions. This work was supported by the U.S. Department of Energy under Contract No. DE-FG02-01ER45910. J.J.H. was supported in part by a Laboratory Directed Research and Development grant from Sandia National Laboratories. Financial support was also provided by the DOE Computational Materials Science Network program.

[1] J. S. Langer, in *Directions in Condensed Matter*, edited by G. Grinstein and G. Mazenko (World Scientific, Singapore, 1986), p. 164.
[2] A. Karma and W.-J. Rappel, Phys. Rev. E **57**, 4323 (1998).
[3] M. Plapp and A. Karma, Phys. Rev. Lett. **84**, 1740 (2000).
[4] N. Provatas, N. Goldenfeld, and J. Dantzig, Phys. Rev. Lett. **80**, 3308 (1998).
[5] A.A. Wheeler, W.J. Boettinger, and G.B. McFadden, Phys. Rev. A **45**, 7424 (1992).
[6] A.A. Wheeler, W.J. Boettinger, and G.B. McFadden, Phys. Rev. E **47**, 1893 (1993).
[7] G. Caginalp and W. Xie, Phys. Rev. E **48**, 1897 (1993).
[8] A. Karma, Phys. Rev. Lett. **87**, 115701 (2001).
[9] J.A. Warren and W.J. Boettinger, Acta Metall. Mater. **43**, 689 (1995).
[10] W.J. Boettinger and J.A. Warren, J. Cryst. Growth **200**, 583 (1999).
[11] W. Losert, D.A. Stillman, H.Z. Cummins, P. Kopczynski, W.-J. Rappel, and A. Karma, Phys. Rev. E **58**, 7492 (1998).
[12] D.I. Meiron, Phys. Rev. A **33**, 2704 (1986).
[13] D.A. Kessler and H. Levine, Phys. Rev. B **33**, 7867 (1986).
[14] D.A. Kessler, J. Koplik, and H. Levine, Adv. Phys. **40**, 255 (1988).
[15] J. Bragard, A. Karma, Y. H. Lee, and M. Plapp, Interface Sci. **10**, 121 (2002).
[16] M.E. Glicksman and N.B. Singh, J. Cryst. Growth **98**, 277 (1989).
[17] M. E. Glicksman and N. B. Singh, in *Rapidly Solidified Powder Aluminum Alloys*, edited by M. E. Fine and E. A. Starke (ASTM, Philadelphia, 1986), p. 44.
[18] M. Muschol, D. Liu, and H.Z. Cummins, Phys. Rev. A **46**, 1038 (1992).
[19] A. Dougherty and J.P. Gollub, Phys. Rev. A **38**, 3043 (1988).
[20] P. Oswald, J. Phys. (France) **49**, 1083 (1988).
[21] K.K. Koo, R. Ananth, and W.N. Gill, Phys. Rev. A **44**, 3782 (1991).
[22] S. Liu, R.E. Napolitano, and R. Trivedi, Acta Mater. **49**, 4271 (2001).
[23] M.S. Daw and M.I. Baskes, Phys. Rev. Lett. **50**, 1285 (1983).
[24] M.S. Daw and M.I. Baskes, Phys. Rev. B **29**, 6443 (1984).
[25] M.S. Daw, S.M. Foiles, and M.I. Baskes, Mater. Sci. Rep. **9**, 251 (1993).
[26] S.M. Foiles, Phys. Rev. B **32**, 3409 (1985).
[27] M.M.G. Alemany, C. Rey, and L.J. Gallego, J. Chem. Phys. **109**, 5175 (1998).
[28] J.J. Hoyt, B. Sadigh, M. Asta, and S.M. Foiles, Acta Mater. **47**, 3181 (1999).
[29] M. Asta, D. Morgan, J.J. Hoyt, B. Sadigh, J.D. Althoff, D. de Fontaine, and S.M. Foiles, Phys. Rev. B **59**, 14 271 (1999).
[30] M.M.G. Alemany, C. Rey, and L.J. Gallego, J. Chem. Phys. **111**, 9111 (1999).
[31] J.J. Hoyt, M. Asta, and B. Sadigh, Phys. Rev. Lett. **85**, 594 (2000).
[32] M. Dzugutov, Nature (London) **381**, 137 (1996).
[33] Y. Rosenfeld, Phys. Rev. A **15**, 2545 (1977).
[34] Y. Rosenfeld, Chem. Phys. Lett. **48**, 467 (1977).
[35] J. J. Hoyt, M. Asta, and A. Karma, Interface Sci. **10**, 181 (2002).
[36] J.Q. Broughton, G.H. Gilmer, and K.A. Jackson, Phys. Rev. Lett. **49**, 1496 (1982).
[37] E. Burke, J.Q. Broughton, and G.H. Gilmer, J. Chem. Phys. **89**, 1030 (1988).
[38] H.E.A. Huitema, M.J. Vlot, and J.P. van der Erden, J. Chem. Phys. **111**, 4714 (1999).
[39] L.A. Baez and P. Clancy, J. Chem. Phys. **102**, 8138 (1995).
[40] W.J. Briels and H.L. Tepper, Phys. Rev. Lett. **79**, 5074 (1978).
[41] H.L. Tepper and W.J. Briels, J. Cryst. Growth **230**, 270 (2001); J. Chem. Phys. **115**, 9434 (2001).
[42] M. Ishimaru, S. Munetoh, T. Motooka, K. Moriguchi, and A. Shintani, Phys. Rev. B **58**, 12 583 (1998).
[43] J. Tersoff, Phys. Rev. B **38**, 9902 (1988).
[44] M.J. Uttormark, M.O. Thompson, and P. Clancy, Phys. Rev. B **47**, 15 717 (1993).
[45] A.P. Horsfield and P. Clancy, Modell. Simul. Mater. Sci. Eng. **2**, 277 (1994).
[46] F.H. Stillinger and T.A. Weber, Phys. Rev. B **31**, 5262 (1985).
[47] C.J. Tymczak and J.R. Ray, Phys. Rev. Lett. **64**, 1278 (1990); J. Chem. Phys. **92**, 7520 (1990).
[48] Q.M. Yu, M.O. Thompson, and P. Clancy, Phys. Rev. B **53**, 8386 (1996).
[49] C.F. Richardson and P. Clancy, Phys. Rev. B **45**, 12 260 (1992).
[50] F. Celestini and J.M. Debierre, Phys. Rev. B **62**, 14 006 (2000).
[51] F. Celestini and J.M. Debierre, Phys. Rev. E **65**, 041605 (2002).
[52] H.E.A. Huitema, B. van Hengstrum, and J.P. van der Erden, J. Chem. Phys. **111**, 10 248 (1999).
[53] J.J. Hoyt, M. Asta, and A. Karma, Phys. Rev. Lett. **86**, 5530 (2001).
[54] J. J. Hoyt, M. Asta, and A. Karma (unpublished).
[55] J. R. Morris, Z. Y. Lu, and K. M. Ho, Interface Sci. **10**, 143 (2002).
[56] J.Q. Broughton and G.H. Gilmer, J. Chem. Phys. **84**, 5759 (1986).
[57] R.L. Davidchack and B.B. Laird, Phys. Rev. Lett. **85**, 4751 (2000).
[58] L. Yang, S. Kado, and G. Derge, Trans. AIME **212**, 628 (1958).
[59] J. H. Hollomon and D. Turnbull, *Progress in Metal Physics* (Pergamon, Oxford, 1953), Vol. 1, p. 356.
[60] D.R.H. Jones, J. Mater. Sci. **9**, 1 (1974).
[61] A.F. Voter and S.P. Chen, in *Characterization of Defects in Materials*, edited by R. W. Siegel and R. Sinclair, MRS Symposia Proceedings No. 82 (Materials Research Society, Pittsburgh, 1978), p. 175.
[62] S.M. Foiles, M.I. Baskes, and M.S. Daw, Phys. Rev. B **33**, 7983 (1986).
[63] M. P. Allen and D. J. Tildesley, *Computer Simulation of Liquids* (Oxford University Press, New York, 1993).
[64] A.F. Voter, Proc. SPIE **821**, 214 (1987).
[65] M.M.G. Alemany, C. Rey, and L.J. Gallego, Phys. Rev. B **58**, 685 (1998).
[66] S.M. Foiles and J.B. Adams, Phys. Rev. B **40**, 5909 (1989).
[67] H.A. Wilson, Philos. Mag. **50**, 238 (1900).
[68] J. Frenkel, Phys. Z. Sowjetunion **1**, 498 (1932).
[69] D. Turnbull, J. Phys. Chem. **66**, 609 (1962).
[70] K. A. Jackson, Interface Sci. **10**, 159 (2002).
[71] The term $e^{-\Delta S/k_B}$ in Eq. (5) does not appear in the original expression of BGJ. It is argued by Jackson (Ref. 70) that this term

should be retained in the general relation for growth velocities. We find slightly better agreement between model and simulation results when this term is retained.
[72] R.H. Ewing, J. Cryst. Growth **11**, 221 (1971).
[73] M. Heni and H. Lowen, Phys. Rev. E **60**, 7057 (1999).
[74] B.B. Laird, J. Chem. Phys. **115**, 2887 (2001).
[75] A. Karma, Phys. Rev. Lett. **70**, 3439 (1993); Phys. Rev. E **48**, 3441 (1993).